

RESEARCH ARTICLE | JUNE 03 2024

Multi-functional gas cell in the vacuum ultraviolet free-electron laser beamline



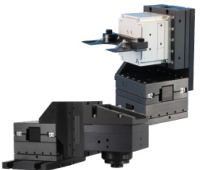
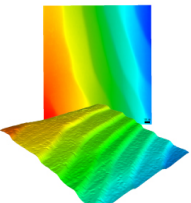
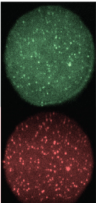
Mingchang Wang ; Yong Yu ; Jiayue Yang ; Qinming Li  ; Weiqing Zhang  



Rev. Sci. Instrum. 95, 063101 (2024)

<https://doi.org/10.1063/5.0202267>



 <p>MCL MAD CITY LABS INC. www.madcitylabs.com</p>	<p>Nanopositioning Systems</p> 	<p>Modular Motion Control</p> 	<p>AFM and NSOM Instruments</p> 	<p>Single Molecule Microscopes</p> 
--	--	--	---	--

Multi-functional gas cell in the vacuum ultraviolet free-electron laser beamline

Cite as: Rev. Sci. Instrum. 95, 063101 (2024); doi: 10.1063/5.0202267

Submitted: 3 February 2024 • Accepted: 11 May 2024 •

Published Online: 3 June 2024



View Online



Export Citation



CrossMark

Mingchang Wang,^{1,2} Yong Yu,³ Jiayue Yang,¹ Qinming Li,^{3,a)} and Weiqing Zhang^{1,a)}

AFFILIATIONS

¹ State Key Laboratory of Molecular Reaction Dynamics, Dalian Institute of Chemical Physics, Chinese Academy of Sciences, 457 Zhongshan Road, Dalian 116023, China

² University of Chinese Academy of Sciences, 1 Yanqihu East Road, Beijing 101408, China

³ Institute of Advanced Science Facilities, 268 Zhenyuan Road, Shenzhen 518107, China

^{a)} Authors to whom correspondence should be addressed: liqinming@mail.iasf.ac.cn and weiqingzhang@dicp.ac.cn.
Tel.: +86-0411-84379867

ABSTRACT

A long gas cell, filled with noble gas, is typically positioned between the undulator and the first mirror in the free-electron laser (FEL) beamline to attenuate the laser power as required by the end-stations. In addition to attenuation, the gas cell also serves important functions in various applications, such as spectrometer calibration, resolving power evaluation during beamline commissioning, and filtering of third harmonic in FEL operations. These functions of the gas cell have been successfully tested and implemented at the Dalian Coherent Light Source, a vacuum ultraviolet FEL facility located in Dalian, China. The resolving power of higher than 5000 has been obtained, and accurate calibration has been completed using the gas cell. During operation, the third harmonic of the FEL was attenuated by approximately one order of magnitude with almost the same power of the fundamental. This greatly improved the signal-to-noise ratio at the end-stations.

Published under an exclusive license by AIP Publishing. <https://doi.org/10.1063/5.0202267>

I. INTRODUCTION

Free-electron Lasers (FELs) exhibit high peak power, narrow bandwidth, and full coherence, making them invaluable in various research domains, including material science, chemical engineering, and biopharmaceutics.¹ The Dalian Coherent Light Source (DCLS),^{2–4} a vacuum ultraviolet (VUV) FEL user facility with an electron beam energy of 300 MeV and a FEL wavelength of 50–150 nm, has been serving the scientific community for more than seven years. At DCLS, the high-gain harmonic generation (HG) lasing mode⁵ is adopted to generate fully coherent FEL pulses with a typical repetition rate of 10 Hz, a pulse duration of 1 ps, and a pulse energy of about 100 μ J. This new light source enables researchers to explore unknown scientific laws. However, it is imperative to elucidate the power-dependent effects before data acquisition to prevent misinterpretation of the results. Manipulating the undulator to adjust the power is not a feasible solution. Therefore, it is essential to integrate an attenuation device in the FEL beamline. All FEL facilities are equipped with a gas cell,^{6–11} which serves as an attenuator when filled with noble gases. In addition to attenuators, we have also

utilized the gas cell for spectrometer calibration, resolving power evaluation,^{12,13} and third harmonic filtering.

Online calibration and resolving power evaluation of a spectrometer are essential in beamline commissioning and experiments^{14,15} that require precise spectral data. Typically, spectrometer calibration employs emission lines from mercury¹⁶ and deuterium lamps,¹⁷ as well as transmission lines from holmium oxide in neodymium filters and 4% holmium oxide in 10% perchloric acid.¹⁸ However, these methods are performed offline, and the intensity of these light sources is insufficient to yield a usable signal for the online spectrometer designed for FEL with high pulse power. Therefore, they are not suitable for online calibration of the spectrometer at DCLS. The absorption lines of noble gases, such as He, Ar, and Kr,¹⁹ can be a suitable method for the calibration of the online spectrometer at DCLS. We can introduce noble gases into the gas cell to produce absorption lines, which allows for simultaneous calibration and resolving power evaluation of the spectrometer.

FEL mixed with third harmonic is catastrophic for many experiments. Although the components of the third harmonics are

approximately one order of magnitude lower than that of the fundamental, their large interaction cross section can still introduce significant noise into the experimental data. To mitigate this issue, various strategies for the filtering of the third harmonic are implemented on the beamline, including solid film filtering²⁰ and front mirror cutoff frequency filtering. However, the database²¹ indicates that there is currently no appropriate material for filtering the third harmonics while maintaining the FEL in the 50–150 nm range using the first two methods. Therefore, the gas cell^{22,23} with noble gases provides an exclusive solution for third harmonic filtering in the VUV band at DCLS. The third harmonic can be suppressed by more than one order of magnitude due to the significant difference in absorption of the FEL and third harmonic. A gas cell uses gas as the working medium instead of a solid filter, making it less susceptible to damage and allowing for long-term operation. This ensures the accuracy and reliability of the data at end-stations. We utilize the multifunctional gas cell to realize the calibration, resolving power test of the spectrometer, and high harmonic filtering at the same time, which provides an important reference for the commission and operation of the beamline.

II. METHODOLOGY

The gas cell situated in the front-end of DCLS is 2000 mm long and has a maximum pressure of 30 Pa at its center. To maintain the

vacuum level of the beamline, six difference pumps (DPs) are positioned on either side of the gas cell. These chambers improve the vacuum level to 5×10^{-7} Pa at the machine and the mirror side. The vacuum pump in the first four chambers at each side are the Pfeiffer Hipace 80 and Hipace 300 turbo pump, with pumping speeds from 70 to 250 l/s. In addition, the vacuum pump in the last two chambers is the Agilent Plus 300 ionic pump, with the pumping speeds of 300 l/s. Stainless steel tubes with a diameter of 20 mm are used to control conductance between two differential pumping stations. Limited by the space at the front-end of the beamline, the Beam-defining Apertures (BDAs) and Beam Position Monitor (BPM) are set in the difference pumps. The Intensity Monitor (IM) is a light intensity detector based on gas ionization, and the nearby chambers are also responsible for the vacuum differential in this region. Figure 1 shows the schematic diagram of the gas cell. The pressure, flow conduction, and pumping speed of the vacuum pump in each part of the gas cell are shown in Table I.

A. Calibration and resolving power evaluation of the online spectrometer

A $30 \times 10 \text{ mm}^2$ sized variable line spacing grating carved on the center of an M2 plane mirror is the diffraction element of an online spectrometer at DCLS, as shown in Fig. 2. In addition to this, the M2 mirror is also responsible for horizontally transmitting the incoming beam from the M1 mirror in the photon beam transmission system.²

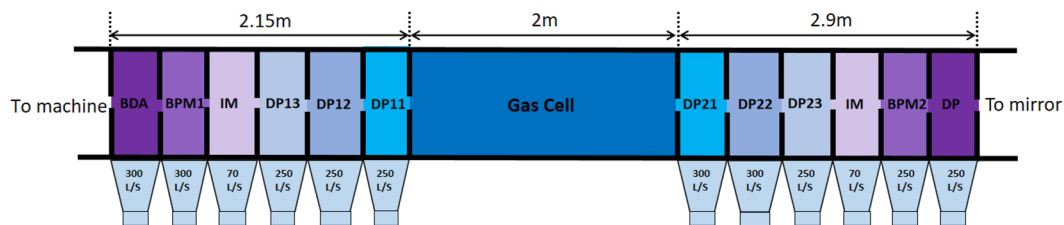


FIG. 1. Schematic diagram of the gas cell and differential system.

TABLE I. Absorption spectral lines selected for calibration.

Chamber	Pump speed/(l/s)	Connecting tube size/cm	Flow conduction/(l/s)	Pressure/Pa
BDA	300	$\varphi = 2; L = 10$	9.68×10^{-1}	5.00×10^{-7}
BPM1	300	$\varphi = 2; L = 15$	6.45×10^{-1}	1.08×10^{-5}
IM	70	$\varphi = 2; L = 25$	3.87×10^{-1}	5.00×10^{-3}
DP13	250	$\varphi = 2; L = 15$	6.45×10^{-1}	2.14×10^{-5}
DP12	250	$\varphi = 2; L = 20$	4.84×10^{-1}	5.30×10^{-3}
DP11	70	$\varphi = 2; L = 50$	1.93×10^2	2.74
GAS CELL	30
DP21	70	$\varphi = 2; L = 50$	1.93×10^2	2.74
DP22	250	$\varphi = 2; L = 20$	4.84×10^{-1}	5.30×10^{-3}
DP23	250	$\varphi = 2; L = 15$	6.45×10^{-1}	2.14×10^{-5}
IM	70	$\varphi = 2; L = 25$	3.87×10^{-1}	5.00×10^{-3}
BPM2	300	$\varphi = 2; L = 50$	1.94×10^{-1}	3.23×10^{-6}
DP	300	$\varphi = 2; L = 50$	1.94×10^{-1}	5.00×10^{-7}

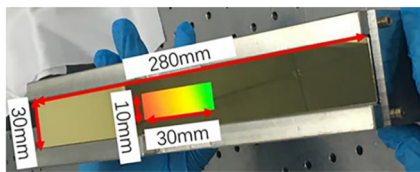


FIG. 2. Physical picture of the sampling grating at the online spectrometer.

When irradiating on the grating, FEL is split into two parts. Over 90% of the zero-order diffraction beam still transports into the end-station, while the first- and higher-order diffraction goes downward at a certain angle into the detector. Based on the detector position, the FEL spectra can be accurately calculated.²⁴ Figure 3 shows the schematic diagram of the relationship between the online spectrometer and gas cell.

Polynomial methods,²⁵ including linear fitting, quadratic polynomial fitting, and others, are the most commonly used calibration methods for spectrometers. The objective functions for fitting are

$$\text{Linear fitting: } \lambda = a_0 + a_1N, \quad (1)$$

$$\text{Quadratic polynomial fitting: } \lambda = a_0 + a_1N + a_2N^2, \quad (2)$$

$$\text{Cubic polynomial fitting: } \lambda = a_0 + a_1N + a_2N^2 + a_3N^3. \quad (3)$$

Suitable polynomials can be selected, and coefficients such as a_0 , a_1 , and a_2 can be obtained by comparing the wavelength of standard spectral lines with their corresponding pixel positions on the spectrometer detector, measured by the linear encoder.

The DCLS wavelength ranges from 50 to 150 nm. To calibrate the spectrometer, seven absorption lines from four noble gases were selected, which are evenly distributed within the 50–150 nm range. Table II shows the characteristic absorption wavelength of the selected gases, according to the database of the National Institute of Standards and Technology (NIST).²⁶

Furthermore, the scanning of the wavelength can be achieved by adjusting the electron beam energy and the undulator gap,²⁷

$$\lambda = \frac{\lambda_u}{2\gamma^2} \left(1 + \frac{K^2}{2} \right), \quad (4)$$

where λ is the wavelength of FEL, λ_u is the undulator period, and K is related to the undulator gap. The Lorentz factor $\gamma = \frac{E}{m_0c^2}$ (E is the energy of the electron beam and m_0c^2 is the rest energy of the electron).

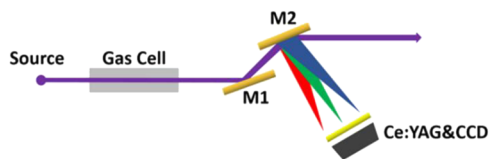


FIG. 3. Schematic diagram of the relationship between the online spectrometer and gas cell.

TABLE II. Absorption spectral lines selected for calibration.

Gas type and energy level	Energy/eV	Wavelength/nm
He 1s2 → 1s2p	21.2742	58.4334
Ne 2s22p6 → 2s22p53s	16.8927	73.5896
Kr 4s24p6 → 4s24p56s	12.4181	100.1060
Kr 4s24p6 → 4s24p55s	10.6718	116.4867
Xe 5p6 → 5p55d	10.4286	119.2037
Xe 5p6 → 5p51/26s	9.5951	129.5588
Xe 5p6 → 5p53/26s	8.4589	146.9610

The bandwidth of FEL is narrower than that of synchrotron radiation, requiring precise adjustment of the wavelength to the absorption peak. The electron beam energy can be adjusted to scan a wide range of wavelengths. When the wavelength coincides with absorption lines, a depletion peak appears in the spectra. This wavelength can be associated with the mechanical position of the detector to calibrate the spectrometer.

The width of the depletion peak results from the resolving power limit of the spectrometer and the convolution of inherent broadening, which includes natural, Doppler, and collisional broadening. Inherent broadening can be calculated, allowing for the evaluation of the spectrometer resolving power.

B. Third harmonic filtering

The third harmonic component is about 1% of the fundamental, and the second harmonic is far less than that of the third harmonic when the FEL is saturated. Therefore, our focus is on filtering out the third harmonics while preserving the fundamental. To achieve this, we have selected two noble gases that satisfy the requirements for third harmonic filtering in the wavelength of DCLS. The transmittance of the fundamental and third harmonic differs by more than one order of magnitude, as shown in Fig. 4. Although Ne can cover a wider range of wavelengths, it requires higher pressure and it is also more expensive. Therefore, the combination of Ne and Ar as the third harmonic filter gases would be

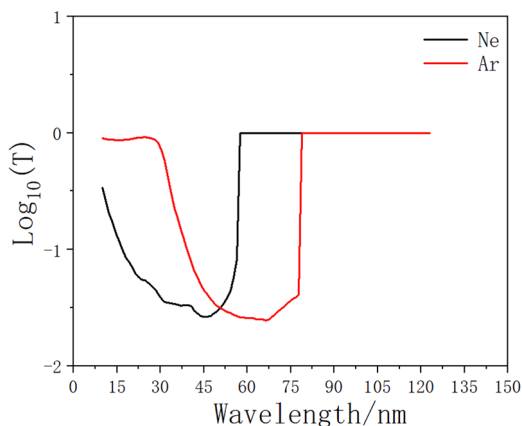


FIG. 4. Transmittance of noble gases at different wavelengths in logarithmic scale.²¹

TABLE III. The gas required for third harmonic filtering.

Fundamental (transparent)/nm	Third harmonic (absorb)/nm	Gas species	Pressure/pa
118–150	39.3–50	Ar	2
58–118	19.3–39.3	Ne	8

more appropriate. Table III shows the gases required for third harmonic filtering at different wavelengths, obtained from the data in Fig. 4 under the pressure conditions that the transmittance of the fundamental and third harmonic differs by more than one order of magnitude.

III. PRELIMINARY RESULTS

A. Calibration and resolving power evaluation of online spectrometer

The pulse energy of FEL in the experiment is about $7 \mu\text{J}$ measured by SXUV100 photodiode manufactured by Opto-Diode Corporation. The pressure in the gas cell was $\sim 1.8 \text{ Pa}$ measured by using the Pfeiffer PKR251 vacuum gauge. The position of the detector was measured using the LIP481R optical encoder manufactured by Dr. Johannes Heidenhain GmbH. The dotted-dashed line in Fig. 5 represents the spectra detected by the spectrometer without filling the gas cell. The spectra with the filled gas cell show clear depletion from absorption, as shown in Fig. 5(a). To acquire the absorption line, we divided the spectra after absorption by the spectra before absorption, as shown in Fig. 5(b).

The online spectrometer calibration was completed after measuring all absorption lines listed in Table II. The calibration result obtained through cubic fitting from the calibration data is $\lambda = 81.849 + 0.434X + 6.213e-4X^2 - 1.208e-7X^3$, as shown in Fig. 6(a). The

fitting residual is shown in Fig. 6(b), and the correlation coefficient R^2 is 0.99999, indicating a good fit to the objective function. Therefore, this formula is the final calibration result for the online spectrometer of DCLS.

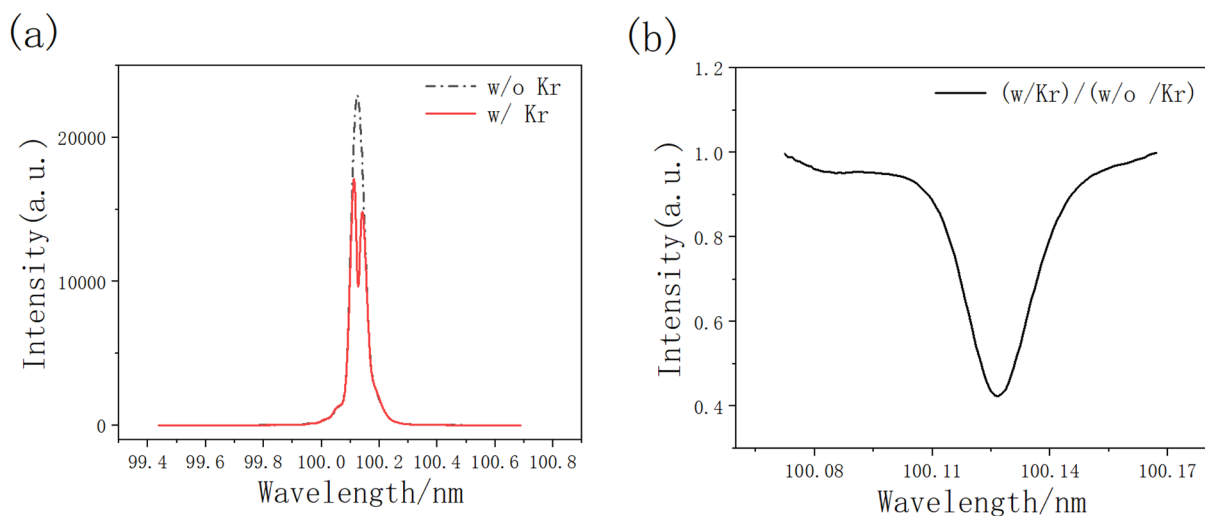
The resolving power of the spectrometer can be evaluated by utilizing Gaussian fitting to obtain the broadening of the absorption line. Figure 7 shows the fitting results selected as examples.

The resolving power of all absorption lines is shown in Table IV. The resolving power is defined as $\lambda/\Delta\lambda$.

The broadening of the absorption line consists of two factors: inherent broadening and the energy resolving power of the spectrometer. Inherent broadening includes natural broadening, Doppler broadening, and collisional broadening. To accurately evaluate the resolving power of the spectrometer, it is imperative to consider the effects of these broadening mechanisms. The results of the spectral line broadening calculations are shown in Table V under 300 K temperature and 2 Pa pressure conditions.

From the data in Table V, the effect of inherent broadening is extremely small and negligible for wavelengths around 100 nm for DCLS.

The simulation results of optical tracing software show that the theoretical resolving power of the spectrometer is about 10000. The disparities between the measured and theoretical values of resolving power in Table IV arise from two primary sources. First, discrepancies between the actual and designed parameters, such as source position, size, and beam divergence, result in the resolving power not fully matching the theory. The second source is that the detector is not precisely located on the focal plane of the spectrometer. The position of the focal plane is theoretically constrained by a trigonometric function, which is not feasible in mechanical design. To align the detector with the focal point, it is moved on a circular guide rail, which introduces defocus. This defocus has a significant impact on resolving power, and actual defocus may be greater due to mechanical installation errors. Future

**FIG. 5.** (a) Raw spectra with and without noble gas, respectively, at 100.106 nm. (b) Absorption line at 100.106 nm.

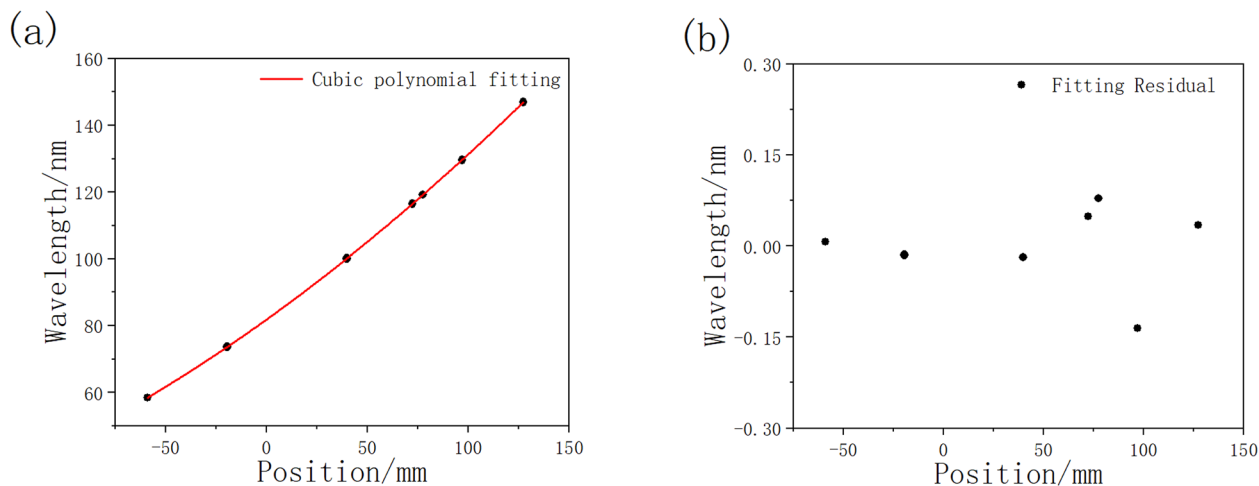


FIG. 6. (a) The calibration curve of the spectrometer. (b) Fitting residual of the calibration curve.

optimization of the spectrometer resolving power can base on this result.

B. Third harmonic filtering

The experiment was conducted using a wavelength of 118.746 nm, which is a commonly used wavelength for end-stations. According to the database,²¹ Ar is a proper gas with the least pressure required for the third harmonic filter. The DCLS spectrometer is designed for the range of 50–150 nm, but the third harmonic of 118.746 nm, which is 39.582 nm, falls out of this range. However, according to grating diffraction theory, FEL at 39.582 nm can be detected by observing its second-order diffraction, which is identical to the first-order diffraction angle for 79.164 nm, as shown in formula (5). The pulse energy of the FEL is approximately 8 μJ. The spectra were collected from 60 to 120 nm with an empty gas cell,

and the results are shown as the red line in Fig. 8. After filling the gas cell with Ar at 2 Pa, it is observed that the fundamental ($M = 1$; $N = 1$) remains almost constant. However, the second harmonic (at 59.373 nm, $M = 2$; $N = 1$) and the second-order diffraction of the third harmonic (at 79.164 nm, $M = 3$; $N = 2$) have been absorbed, as shown in Fig. 8. In this context, M represents the diffraction order and N denotes the harmonic order,

$$\sin \alpha + \sin \beta = nM\lambda, \quad (5)$$

where λ is the wavelength of FEL; α and β are the incidence angle and diffraction angle; n is the grating line density; and M is the diffraction order.

The third harmonic component in FEL is theoretically around 1% of the fundamental, while the second harmonic content is ~0.1%. Figure 8 shows that the intensity of the third harmonic is slightly lower than that of the second harmonic. This discrepancy can be attributed to the lower second-order diffraction efficiency (0.0135%) compared to the first-order diffraction efficiency (0.362%). After

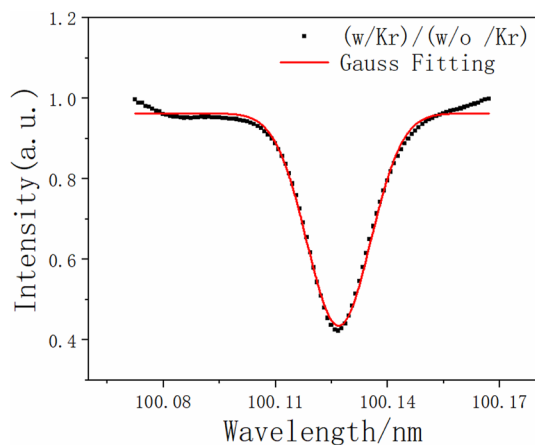


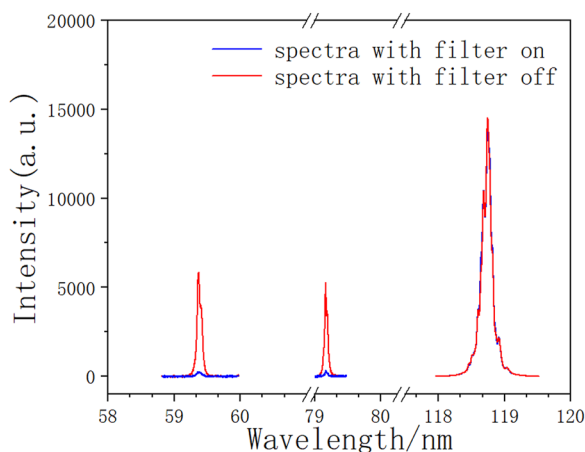
FIG. 7. Gaussian fitting of the absorption line at 100.106 nm.

TABLE IV. Resolving power measurement results.

Gas type and energy level	Absorption peak/nm	Fitting FWHM/nm	Measurement value
He $1s^2 \rightarrow 1s2p$	58.4334	0.014 85	3935
Ne $2s^2 2p^6 \rightarrow 2s^2 2p^5 3s$	73.5896	0.012 32	5973
Kr $4s^2 4p^6 \rightarrow 4s^2 4p^5 6s$	100.1060	0.017 00	5889
Kr $4s^2 4p^6 \rightarrow 4s^2 4p^5 5s$	116.4867	0.025 54	4561
Xe $5p^6 \rightarrow 5p^5 5d$	119.2037	0.023 16	5147
Xe $5p^6 \rightarrow 5p^5_{1/2} 6s$	129.5588	0.027 18	4767
Xe $5p^6 \rightarrow 5p^5_{3/2} 6s$	146.9610	0.032 55	4515

TABLE V. Noble gases absorption line broadening calculation.²⁸

Gas type and energy level	Natural broadening/nm	Doppler broadening/nm	Collisional broadening/nm
He $1s^2 \rightarrow 1s2p$	3.3×10^{-6}	7.6×10^{-10}	3.6×10^{-4}
Ne $2s^2 2p^6 \rightarrow 2s^2 2p^5 3s$	1.7×10^{-6}	6.6×10^{-10}	4.6×10^{-4}
Kr $4s^2 4p^6 \rightarrow 4s^2 4p^5 6s$	1.8×10^{-6}	1.0×10^{-9}	6.2×10^{-4}
Kr $4s^2 4p^6 \rightarrow 4s^2 4p^5 5s$	2.2×10^{-6}	1.4×10^{-9}	7.2×10^{-4}
Xe $5p^6 \rightarrow 5p^5 5d$	4.7×10^{-6}	1.3×10^{-9}	7.4×10^{-4}
Xe $5p^6 \rightarrow 5p^5_{1/2} 6s$	2.2×10^{-6}	1.6×10^{-9}	8.0×10^{-4}
Xe $5p^6 \rightarrow 5p^5_{3/2} 6s$	3.2×10^{-6}	2.0×10^{-9}	9.1×10^{-4}

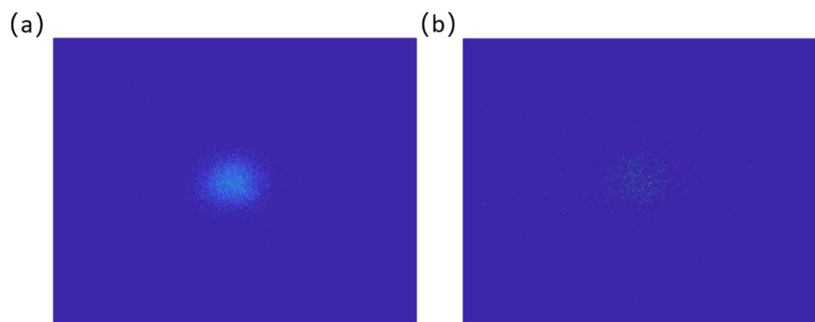
**FIG. 8.** Comparison of the FEL and its higher harmonic intensity with filter on and off.

considering the diffraction efficiency, the intensity of the third harmonic is ~ 12.9 times greater than that of the second harmonic, which is consistent with the theory.

The spectra show negligible attenuation of the fundamental. The intensity of the second harmonic is reduced to 3.97% of

its original value, and the third harmonic is reduced to 5.04%. These results demonstrate the effectiveness of the gas cell in filtering higher-order harmonics while preserving the intensity of the fundamental.

The implementation of the filter has significantly improved the signal-to-noise ratio at the end-station. For instance, the ion imaging end-station uses time-slice ion imaging techniques to investigate chemical reaction mechanism.¹⁵ Chemical reactions $F + CH_4 \rightarrow HF + CH_3$ are used as an example. In this experiment, FEL was set to 120 nm (10.33 eV) to ionize the CH_3 species while avoiding ionization of the CH_4 reactant with ionization thresholds of 9.84 and 12.61 eV. This was done to ensure a good signal-to-noise ratio of the CH_3 product. However, substantial noise from CH_4^+ was observed when injecting CH_4 into the chamber. It should be noted that, from the perspective of ionization energies, the FEL should be incapable of ionizing CH_4 . The noise in this experiment arises from the ionization of the high concentration CH_4 reactant by the third harmonic FEL (31 eV). Figure 9(a) shows that the detector acquires substantial background signals, which pose a significant risk of overwhelming the actual reaction signals. Therefore, it is imperative to mitigate the impact of background signals induced by the third harmonic components. When the gas cell pressure was adjusted to 2 Pa, the background signal reduced dramatically from 10 698 to 548 photons/s, as shown in Fig. 9(b). These findings demonstrate the significance of the gas cell.

**FIG. 9.** Comparison of background signals with the filter off (a) and on (b).

IV. CONCLUSION

A gas cell used to attenuate laser power is the key equipment for the photon beamline. In addition to the attenuation function, we have explored various capacities. By utilizing atomic absorption spectral lines, we have achieved precise calibration and obtained a resolving power surpassing 5000. Taking into account the broadening of the absorption lines, this method is capable of accomplishing high-precision measurements for spectrometers with a resolving power of 100 000 and less. In terms of third harmonic filtering, the gas cell has effectively mitigated the third harmonic of the FEL by approximately one order of magnitude while preserving the intensity of the fundamental. This improves the signal-to-noise ratio by one order of magnitude according to the experiment. In addition, we are also actively exploring the use of the pulse valve instead of leak valve for more efficient high harmonic filtering, which will be further tested in the future. We used the multifunctional gas cell for spectrometer calibration, resolving power testing, and high harmonic filtering simultaneously. It has been experimentally tested and proved to be powerful in beamline commissioning and FEL operation.

ACKNOWLEDGMENTS

The authors are very grateful for the support from Professor Qiu-Ping Wang and Xue-Wei Du, University of Science and Technology of China, on the design of the online spectrometer in DCLS. This work was financially supported by the Shenzhen Science and Technology Program (Grant No. RCBS20221008093327057), the China postdoctoral Science Foundation (Grant No. 2022M713081), the National Key R&D Program of China (Grant No. 2018YFE0203000), the National Natural Science Foundation of China (Grant Nos. 22303055 and 22288201), and the Scientific Instrument Developing Project of Chinese Academy of Science (Grant No. GJJSTD20190002). The authors are very grateful for the support by the technical staff of DCLS.

AUTHOR DECLARATIONS

Conflict of Interest

The authors have no conflicts to disclose.

Author Contributions

M.W. and Y.Y. contributed equally to this work.

Mingchang Wang: Data curation (equal); Formal analysis (equal); Investigation (equal); Methodology (equal); Writing – original draft (equal). **Yong Yu:** Data curation (equal); Formal analysis (equal); Investigation (equal); Methodology (equal); Validation (equal). **Jiayue Yang:** Project administration (equal); Supervision (equal); Validation (equal); Visualization (equal); Writing – review & editing (equal). **Qinming Li:** Data curation (equal); Investigation (equal); Methodology (equal); Supervision (equal); Writing – review & editing (equal). **Weiqing Zhang:** Conceptualization (equal); Funding acquisition (equal); Project administration (equal);

Supervision (equal); Validation (equal); Writing – review & editing (equal).

DATA AVAILABILITY

The data that support the findings of this study are available from the corresponding authors upon reasonable request.

REFERENCES

- 1 P. G. O'Shea and H. P. Freund, *Science* **292**(5523), 1853–1858 (2001).
- 2 Q. Li, Y. Yu, J. Yang, H. Ding, L. Shi, K. Tao, G. Wang, G. Wu, D. Dai, and W. Zhang, in *X-Ray Free-Electron Lasers: Advances in Source Development and Instrumentation* (SPIE, 2019), Vol. 11038, pp. 78–83.
- 3 Y. Yu, Q. Li, J. Yang *et al.*, *Chin. J. Lasers* **46**(1), 0100005 (2019).
- 4 J. Sun, X. Li, J. Yang *et al.*, *Nucl. Instrum. Methods Phys. Res., Sect. A* **1063**, 169320 (2024).
- 5 L. H. Yu, M. Babzien, I. Ben-Zvi *et al.*, *Science* **289**(5481), 932–934 (2000).
- 6 E. Allaria, C. Callegari, D. Cocco, W. M. Fawley, M. Kiskinova, C. Masciovecchio, and F. Parmigiani, *New J. Phys.* **12**(7), 075002 (2010).
- 7 S. Moeller, J. Arthur, A. Brachmann, R. Coffee, F.-J. Decker, Y. Ding, D. Dowell, S. Edstrom, P. Emma, and Y. Feng, *Nucl. Instrum. Methods Phys. Res., Sect. A* **635**(1), S6–S11 (2011).
- 8 S. Owada, K. Togawa, T. Inagaki, T. Hara, T. Tanaka, Y. Joti, T. Koyama, K. Nakajima, H. Ohashi, and Y. Senba, *J. Synchrotron Radiat.* **25**(1), 282–288 (2018).
- 9 Z. Zhao, D. Wang, Q. Gu, L. Yin, G. Fang, M. Gu, Y. Leng, Q. Zhou, B. Liu, and C. Tang, *Synchrotron Radiat. News* **30**(6), 29–33 (2017).
- 10 U. Hahn and K. Tiedtke, *AIP Conf. Proc.* **879**, 276–282 (2007).
- 11 K. Tiedtke, A. Azima, N. von Bargen *et al.*, *New J. Phys.* **11**, 023029 (2009).
- 12 N. Gerasimova, S. Dziarzhytski, and J. Feldhaus, *J. Mod. Opt.* **58**(16), 1480–1485 (2011).
- 13 N. Gerasimova, D. La Civita, L. Samoylova *et al.*, *J. Synchrotron Radiat.* **29**(5), 1299–1308 (2022).
- 14 G. Wu, W. Zhang, H. Pan, Q. Shuai, B. Jiang, D. Dai, and X. Yang, *Rev. Sci. Instrum.* **79**(9), 094104 (2008).
- 15 Y. Chang, Y. Yu, F. An, Z. Luo, D. Quan, X. Zhang, X. Hu, Q. Li, J. Yang, and Z. Chen, *Nat. Commun.* **12**(1), 2476 (2021).
- 16 C. J. Sansonetti, M. L. Salit, and J. Reader, *Appl. Opt.* **35**(1), 74–77 (1996).
- 17 L. Carraro, M. Cortiana, M. E. Puiatti, F. Sattin, P. Scarin, and M. Valisa, *Rev. Sci. Instrum.* **66**(1), 613–615 (1995).
- 18 K. Liu and F. Yu, *Opt. Eng.* **52**(1), 013603 (2013).
- 19 X. Wang, M. Chini, Y. Cheng, Y. Wu, and Z. Chang, *Appl. Opt.* **52**(3), 323–329 (2013).
- 20 K. Jimenez, P. Nicolosi, L. Juschkun, N. Ahmed, A. E. H. Gaballah, E. Cattaruzza, M. G. Sertsu, A. Gerardino, A. Giglia, G. Mussler, and P. Zuppella, *Thin Solid Films* **695**, 137739 (2020).
- 21 B. L. Henke, E. M. Gullikson, and J. C. Davis, *At. Data Nucl. Data Tables* **54**(2), 181–342 (1993).
- 22 B. Mercier, M. Compin, C. Prevost, G. Bellec, R. Thissen, O. Dutuit, and L. Nahon, *J. Vac. Sci. Technol. A* **18**(5), 2533–2541 (2000).
- 23 M. Johnson, A. Bodi, L. Schulz, and T. Gerber, “Vacuum ultraviolet beamline at the Swiss Light Source for chemical dynamics studies,” *Nucl. Instrum. Methods Phys. Res., Sect. A* **610** (2), 597–603 (2009).
- 24 C. Li, S. Wei, X. Du, L. Du, Q. Wang, W. Zhang, G. Wu, D. Dai, and X. Yang, *Nucl. Instrum. Methods Phys. Res., Sect. A* **783**, 65–67 (2015).
- 25 G. Xiong, J. Zhang, G. Yang, J. Yang, H. Li, Z. Hu, Y. Zhao, M. Wei, and T. Yi, *Phys. Scr.* **89**(6), 065005 (2014).
- 26 A. Kramida, Y. Ralchenko, and J. Reader, *Atomic Spectra Database, NIST Standard Reference Database*, 2022.
- 27 S. Khan, “Free-electron lasers,” *J. Mod. Opt.* **55**, 3469–3512 (2008).
- 28 W. Demtröder, *Laser Spectroscopy I: Basic Principles* (Springer, 2014).